Workability studies of sintered aluminium composites during hot deformation

Sumesh Narayan and Ananthanarayanan Rajeshkannan

Proceedings of the Institution of Mechanical Engineers, Part B: Journal of Engineering Manufacture published online 27 November 2014
DOI: 10.1177/0954405414556497

Original Article

Institution of MECHANICAL ENGINEERS
Journal of ENGINEERING MANUFACTURE

Proc IMechE Part B:
J Engineering Manufacture
1–11

DOI: 10.1177/0954405414556497
pib.sagepub.com
SAGE

Workability studies of sintered aluminium composites during hot deformation

Sumesh Narayan and Ananthanarayanan Rajeshkannan

Abstract

Experimental investigation has been carried out to evaluate the effect of titanium carbide (TiC), molybdenum carbide (Mo_2C), iron carbide (Fe_3C) and tungsten carbide (WC) addition on the composite aluminium preforms. The hot upsetting of the composite aluminium preforms with various carbide contents, namely, Al-4% TiC, Al-4% WC, Al-4% Fe_3C and Al-4% Mo_2C, and different aspect ratios, namely, 0.4 and 0.6, was carried out and the workability behaviour of the same was determined. The influence of carbide addition in the aluminium composite and initial preform geometry on the relative density (R), stress ratio parameters, $\sigma_\theta/\sigma_{eff}$, σ_m/σ_{eff} and σ_z/σ_{eff}, and formability stress index was studied.

Keywords

Metal matrix composites, plastic deformation, porosity, powder processing

Date received: 1 April 2014; accepted: 22 September 2014

Introduction

Powder metallurgy (P/M) manufacturing route is used for mass production of precision engineering materials as its ability to produce complex parts with close tolerances and with maximum material utilization. Aluminium metal matrix composites (MMCs) are used for wide variety of industrial applications due to its unique properties such as low specific density, high strength, low thermal expansion and good wear resistance and are economically viable.[1–5] Ductile aluminium matrix reinforced with stronger and stiffer carbides provides a combination of properties of the metallic material and ceramic reinforcement components.[6] Titanium carbide (TiC) and tungsten carbide (WC)–based composites are currently used in high-strength application where improved strength, wear resistance and corrosion resistance are required[7,8] and aluminium reinforced with WC prepared via warm accumulative roll bonding process showed improved mechanical properties.[9] One of the simplest secondary processes used by many researchers[10–12] is open die forging of cylindrical billets. The residual porosity left in the part causes the failure (visible cracks appearing on the free surface) in the compacts during open die forging and, hence the workability of the materials needs to be studied.

The workability or formability of the P/M material plays a major role in determining whether the P/M material will be formed successfully or fracture initiates in the forming process. Workability is a measure of the extent of deformation that a material can withstand due to the induced internal stresses of forming prior to fracture and is not only dependent on the material but also on several forming parameters such as stress and strain rates, friction and temperature.[13–15] Many researchers[16–20] have studied hot formability of aluminium MMC where the constitutive equations related to flow stress, temperature, strain rate and flow strain. Kuhn and Downey[21] proposed a plasticity theory relating yield stress and deformed density by studying the deformation behaviour and the plasticity theory of some sintered P/M materials via open die forging.

A plasticity theory proposed by Shima and Oyane[22] and Green[23] has been utilized to study workability and deformation behaviour considering numerous spherical cracks and voids, stress in the direction of compression and relative density. Narayanasamy et al.[24–26] studied the fracture criterion of porous materials under plane

Mechanical Engineering, School of Engineering and Physics, Faculty of Science, Technology and Environment, The University of the South Pacific, Suva, Fiji

Corresponding author:
Sumesh Narayan, Mechanical Engineering, School of Engineering and Physics, Faculty of Science, Technology and Environment, The University of the South Pacific, Laucala Campus, P.O. Box 1168, Suva, Fiji.
Email: narayan_su@usp.ac.fj

Table 1. Sieve size analysis of aluminium powder.

Sieve size (μm)	250	+200	+150	+100	+75	+45	−45
Retention in sieve (weight %)	0.2	0.3	16.3	55.3	9.5	7.9	10.5

Table 2. Characterization of aluminium powder and its blends.

Property	Al	Al-4% WC	Al-4% TiC	Al-4% Fe_3C	Al-4% Mo_2C
Apparent density (g/cm^3)	1.091	1.345	1.186	1.308	1.325
Flow rate (s/50 g) by hall flow meter	87.306	79.647	85.202	80.559	80.481
Compressibility (g/cm^3) at pressure of 130 ± 10MPa	2.356	2.113	2.280	2.235	2.210

stress state, uniaxial stress state and triaxial stress state conditions relating hoop stress, mean stress, effective stress and the several stress ratio parameters. One of the most important parameters in the study of workability characteristics is the formability stress index proposed by Abdel-Rahman and El-Sheikh.[14] It describes the effect of hydrostatic stress and the effective stress on the P/M compacts. Vujovic and Shabaik[27] and Doraivelu et al.[28] proposed a new yield criterion for porous material validating it using experiments and simulations. Ko et al.[29] studied the microstructure and hot workability of SiC_p/AA 2024 composite and reported that dynamic recrystallization was responsible for the hot restoration of the composites. Furthermore, they reported upon increasing the SiC_p volume fraction, the flow stress increased and the failure strain decreased.

Narayanasamy et al.[30] studied hot forging of P/M sintered high-strength 4% TiC composite steel preforms under different stress state conditions proposing a new geometrical shape factor and exponential relationship between the relative density ratio and hoop strain. It was reported that a straight line relationship was established between relative density against new geometrical shape factor and respective stress ratio parameters. Rajeshkannan[12] studied workability of sintered copper alloy preforms during cold upsetting using different curve fitting techniques and reported that decreasing aspect ratio facilitated deformation and improved the formability stress index; however, it limited height strain to fracture. Similar study was carried out by Narayanasamy et al.[31] via hot forging of 4% TiC composite steel preforms and similar results were reported. Taha et al.[11] presented some experimental data on workability of aluminium particulate–reinforced MMCs prepared by stir-casting, squeeze-casting and P/M techniques. They reported that the workability of aluminium SiC- and Al_2O_3-reinforced MMCs is affected positively by the following: applying intermediate heat treatment, decreasing particulate volume fraction, decreasing particulate size and reinforcing with SiC in a wrought alloy matrix rather than Al_2O_3.

The residual porosity left in the P/M parts after the primary P/M process is a major drawback and these residual porosities are the main cause of failure during the secondary process and, hence workability studies are important in the preform geometry design and die constraint designs. Thus, the present investigation is aimed to establish the workability limit under triaxial stress state condition of P/M preforms of Al-4% TiC, Al-4% iron carbide (Fe_3C), Al-4% WC and Al-4% molybdenum carbide (Mo_2C) (weight percentage) experimentally and to establish the technical relationship that exists between the characteristics of axial stress, hoop stress, hydrostatic stress, effective stress and formability stress index with respect to true height strain and densification.

Experimental details

Materials and characteristics

Aluminium powder of less than or equal to 150 μm in size (diameter) and respective carbide powders, namely, TiC, WC, Mo_2C and Fe_3C, of less than or equal to 50 μm in size (diameter) was used in this experiment. The basic characterization of elemental aluminium powder such as flow rate, apparent density, compressibility and sieve analysis has been carried out using standard methods of testing. The characteristics are given in Tables 1 and 2, respectively.

Powder blending and compaction

The required mass of aluminium and respective carbide powders was accurately weighed and mixed to obtain Al-4% TiC, Al-4% WC, Al-4% Fe_3C and Al-4% Mo_2C in a ball milling machine with powder mixed to stainless steel balls (10 mm inner diameter) with a ratio of 1:1 by weight. Air tight containers were used here to avoid oxidation of aluminium powders. The ball mill was operated for 10 h at 200 r/min to get a homogenized mixture. The apparent density was measured at 1-h interval to ensure homogeneous mixture was obtained. Towards the end of blending process, a consistent apparent density ensured homogeneous mix. The blended powders were then compacted using 100 ton capacity hydraulic press into cylindrical billets of aspect ratio (height-to-diameter ratio) of 0.4 and 0.6. The respective compacting pressures were obtained from the

compressibility curve prepared for each material so as to obtain an initial theoretical density of 0.86 ± 0.01. Initial theoretical density is the initial density of the preform divided by 100% density of the preform (no pores).

Ceramic coating, drying and sintering

Immediately after compaction, an indigenously developed ceramic coating was applied on the compacts. This coating was allowed to dry for a period of 12 h at normal atmospheric conditions. Recoating was employed to the preforms in the direction 90° to that of the earlier coating. Again the compacts were allowed to dry for a period of 12 h. The coating was applied to avoid oxidation of compacts during the sintering process. The ceramic-coated compacts were sintered in an electric muffle furnace at a temperature of 220 °C for 30 min (drying process) and then at the temperature of 594 °C for further 60 min.

Hot deformation and measurements

Hot upsetting of the sintered preforms followed immediately after the sintering process at a temperature of 594 °C to the different levels of height strain. The forging operation was carried out with no lubricant. Dimensional measurements such as deformed height (h_f) and deformed diameters, namely, contact diameter at the top surface (D_{c1}), contact diameter at the bottom surface (D_{c2}) and bulged diameter (D_b), were carried out after every step of deformation. The density measurements of the forged specimens were carried out using Archimedes principle. Experimental data were used to calculate the stress ratio parameters, namely ($\sigma_\theta/\sigma_{eff}$), ($\sigma_m/\sigma_{eff}$) and ($\sigma_z/\sigma_{eff}$), axial strain, true diameter strain, percent relative density, actual bulged length and formability stress index.

Theoretical analysis

Using the mathematical expressions, the various upsetting parameters that influence workability characteristics of the selected composite were determined and presented here. The state of stress in a homogeneous compression process is as follows: according to Abdel-Rahman and El-Sheikh[14]

$$\sigma_z = \frac{load}{contact\ surface\ area} = -\sigma_{eff},\ \sigma_r = \sigma_\theta = 0 \tag{1}$$

$$\sigma_m = \left(\frac{\sigma_z}{3}\right) = -\left(\frac{\sigma_{eff}}{3}\right) \tag{2}$$

and the expression for the axial strain can be written as follows

$$\varepsilon_z = -\varepsilon_{eff} = \ln\left(\frac{h_f}{h_o}\right) \tag{3}$$

and true hoop strain is

$$\varepsilon_\theta = \varepsilon_r = \ln\left(\frac{D_f}{D_o}\right) \tag{4}$$

where h_o is the initial height of the preform, h_f the forged height of the preform, D_f the contact diameter after deformation of the preform and D_o the initial diameter of the preform.

According to Narayanasamy et al.,[13,32] the hoop strain under plane stress state which includes the forged bulged diameter (D_b) and forged contact diameter (D_c) can be expressed as follows

$$\varepsilon_\theta = \ln\left[\frac{2D_b^2 + D_c^2}{3D_o^2}\right] \tag{5}$$

Plastic deformation of P/M materials is effected by the residual pores and the analysis of such materials requires an appropriate yield criterion which should take the pore effect into account. Many researchers over the years have analysed several different yield criteria for sintered powder materials and a typical theorem is that the plastic deformation occurs when the elasticity strain energy reaches a critical value.[33–35] The formulation can be written as

$$AJ'_2 + BJ_1^2 = Y^2 = \delta Y_0^2 \tag{6}$$

where A, B and δ are yield criterion parameters and are functions of relative density, J_1 is the first invariant of the stress tensor, J'_2 is the second invariant of the stress deviator and Y_0 and Y are yield strength of a solid and partially dense material having relative density R, respectively.[35] The parameters J_1 and J'_2 in the cylindrical coordinate system where the axis represents radial, circular and axial direction can be expressed as follows

$$J'_2 = \frac{1}{6}\left[(\sigma_r - \sigma_\theta)^2 + (\sigma_\theta - \sigma_z)^2 + (\sigma_z - \sigma_r)^2\right] \tag{7}$$

$$J_1 = \sigma_r + \sigma_\theta + \sigma_z \tag{8}$$

Here, for axisymmetric forging, $\sigma_r = \sigma_\theta$, J'_2 and J_1^2 can be written as

$$J'_2 = \frac{1}{6}\left(2\sigma_\theta^2 + 2\sigma_z^2 - 4\sigma_\theta\sigma_z\right) \tag{9}$$

$$J_1^2 = 4\sigma_\theta^2 + \sigma_z^2 + 4\sigma_\theta\sigma_z \tag{10}$$

Substituting equations (9) and (10) into equation (6) gives

$$\frac{A}{6}\left(2\sigma_\theta^2 + 2\sigma_z^2 - 4\sigma_\theta\sigma_z\right) + B\left(4\sigma_\theta^2 + \sigma_z^2 + 4\sigma_\theta\sigma_z\right) = \delta Y_0^2 \tag{11}$$

Qin and Hua[33] have investigated and compared several yield criterion parameters based on plastic Poisson's ratio, relative density and flow stress of the matrix material by previous researchers. The following yield criteria parameters are chosen in this research as

$A = 2 + R^2$, $B = (1 - R^2)/3$ and $\delta = 2R^2 - 1$. Equation (11) can now be written as

$$Y_0 = \sigma_{eff} = \left[\frac{\left(\sigma_z^2 + 2\sigma_\theta^2 - R^2(\sigma_\theta^2 + 2\sigma_\theta\sigma_z)\right)}{2R^2 - 1}\right]^{0.5} \quad (12)$$

Equation (12) gives the expression for effective stress in terms of cylindrical coordinates and can be expressed in another form as

$$\frac{\sigma_{eff}}{\sigma_z} = \left[\frac{1 + 2(\sigma_\theta/\sigma_z)^2 - R^2\left(2(\sigma_\theta/\sigma_z) + (\sigma_\theta/\sigma_z)^2\right)}{2R^2 - 1}\right]^{0.5} \quad (13)$$

According to Narayanasamy et al.,[25] the state of stress in a triaxial stress condition is given by

$$\alpha = \frac{d\varepsilon_\theta}{d\varepsilon_z} = \frac{(2 + R^2)\sigma_\theta - R^2(\sigma_z + 2\sigma_\theta)}{(2 + R^2)\sigma_z - R^2(\sigma_z + 2\sigma_\theta)} \quad (14)$$

Using equation (14) for the values of Poisson's ratio (α), relative density (R) and axial stress (σ_z), the hoop stress (σ_θ) under triaxial stress state condition can be determined as follows

$$\sigma_\theta = \left[\frac{2\alpha + R^2}{2 - R^2 + 2R^2\alpha}\right]\sigma_z \quad (15)$$

where $\alpha = d\varepsilon_\theta/d\varepsilon_z$

Furthermore, rearranging equation (15)

$$\frac{\sigma_\theta}{\sigma_z} = \left[\frac{2\alpha + R^2}{2 - R^2 + 2R^2\alpha}\right] \quad (16)$$

Under triaxial stress state cylindrical coordinates, the hydrostatic stress can be written as follows assuming $\sigma_\theta = \sigma_r$

$$\sigma_m = \frac{\sigma_r + \sigma_\theta + \sigma_z}{3} = \frac{2\sigma_\theta + \sigma_z}{3} \quad (17)$$

Furthermore, rearranging equation (17)

$$\frac{\sigma_m}{\sigma_z} = \frac{1}{3}\left(1 + \frac{2\sigma_\theta}{\sigma_z}\right) \quad (18)$$

The stress formability factor under triaxial stress state condition is given as

$$\beta = 3\left[\frac{(\sigma_m/\sigma_z)}{(\sigma_{eff}/\sigma_z)}\right] \quad (19)$$

The stress formability factor as expressed in equation (19) is used to describe the effect of mean stress and the effective stress on the forming limit of P/M compacts in upsetting.

Results and discussion

A plot has been presented as shown in Figure 1 between axial strain and relative density for two different initial aspect ratios (height-to-diameter ratio of preforms), namely, 0.40 and 0.60, these plots being drawn for initial relative density of 86%. Relative density is the instantaneous density of the preform divided by 100% density of the preform (no pores).

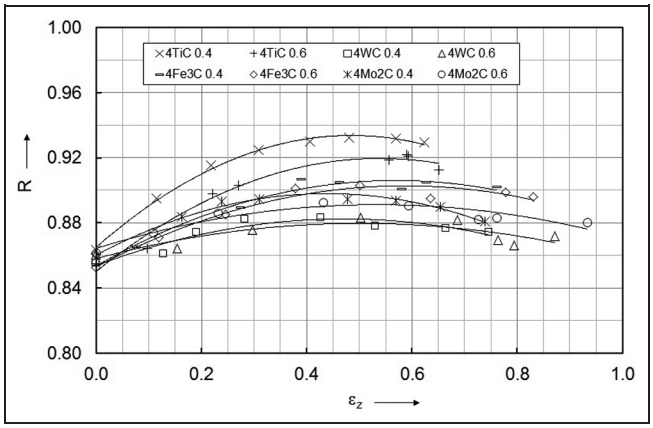

Figure 1. Relationship between relative density and axial strain during hot deformation.

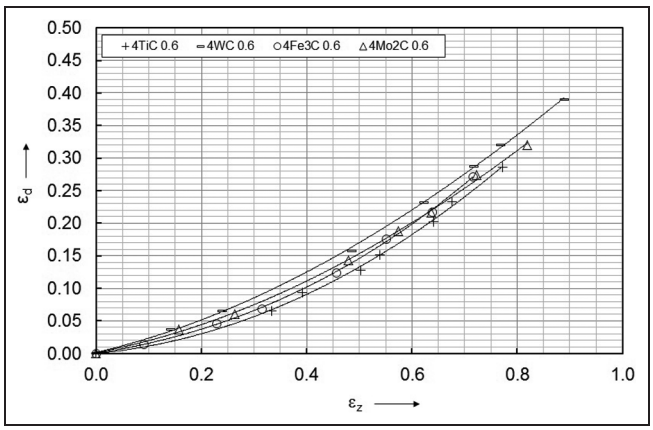

Figure 2. Variation in the diameter strain with respect to the axial strain during hot deformation.

As seen in Figure 1, the relative density increases up to 0.45 axial strain, and thereafter relative density is almost constant till 0.60 axial strain. Then the relative density slightly lowers towards the final stages of deformation. The slight dip in relative density is more evident in Al-4% WC composite. Lower aspect ratio preforms showed better densification in comparison to higher aspect ratio due to the presence of lower pore bed height in the lower aspect ratio preforms. TiC-reinforced aluminium showed better densification rate and better final density achieved followed by Fe_3C-reinforced aluminium and then Mo_2C-reinforced aluminium. WC-reinforced aluminium had the lowest densification rate and final density achieved. However, an inverse relationship exists between densification and fracture strain for the respective composites.

Furthermore, a plot has been presented as shown in Figure 2 between diametrical strain and axial strain for two different initial aspect ratios, namely, 0.40 and 0.60, these plots being drawn for initial relative density

Table 3. Polynomial curve fitting result –*R* versus ε_z.

Al-4TiC	0.4	$R = -0.2922\varepsilon_z^2 + 0.2834\varepsilon_z + 0.8650$	$R_c^2 = 0.9958$
	0.6	$R = -0.2395\varepsilon_z^2 + 0.2579\varepsilon_z + 0.8578$	$R_c^2 = 0.9905$
Al-4Mo_2C	0.4	$R = -0.1966\varepsilon_z^2 + 0.1725\varepsilon_z + 0.8602$	$R_c^2 = 0.9970$
	0.6	$R = -0.0941\varepsilon_z^2 + 0.1006\varepsilon_z + 0.8643$	$R_c^2 = 0.9974$
Al-4Fe_3C	0.4	$R = -0.1617\varepsilon_z^2 + 0.1843\varepsilon_z + 0.8535$	$R_c^2 = 0.9908$
	0.6	$R = -0.1447\varepsilon_z^2 + 0.1697\varepsilon_z + 0.8539$	$R_c^2 = 0.9930$
Al-4WC	0.4	$R = -0.1294\varepsilon_z^2 + 0.1218\varepsilon_z + 0.8538$	$R_c^2 = 0.9935$
	0.6	$R = -0.0859\varepsilon_z^2 + 0.0861\varepsilon_z + 0.8588$	$R_c^2 = 0.9957$

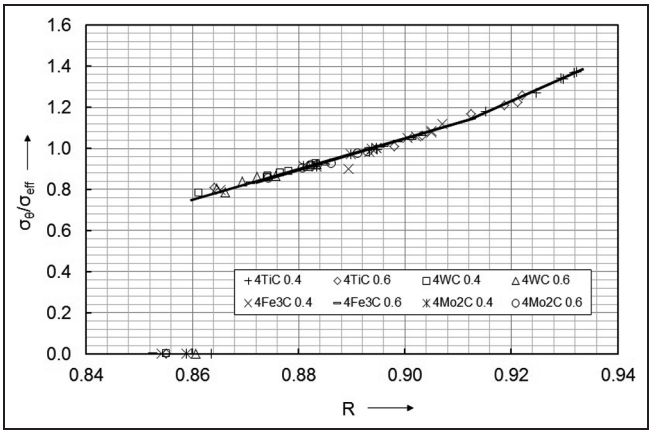

Figure 3. Relationship between stress ratio ($\sigma_\theta/\sigma_{eff}$) and relative density during hot deformation.

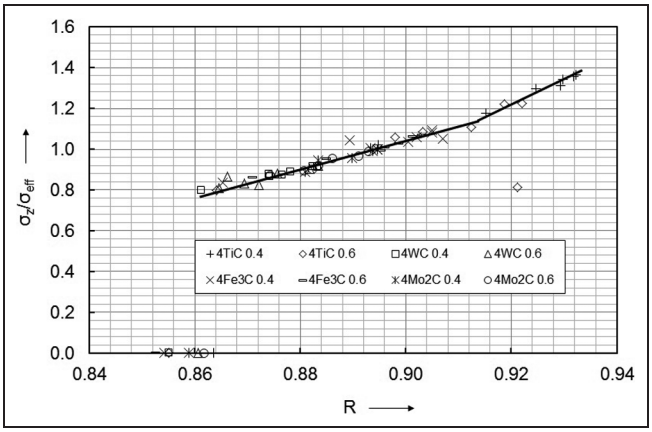

Figure 5. Relationship between stress ratio (σ_z/σ_{eff}) and relative density during hot deformation.

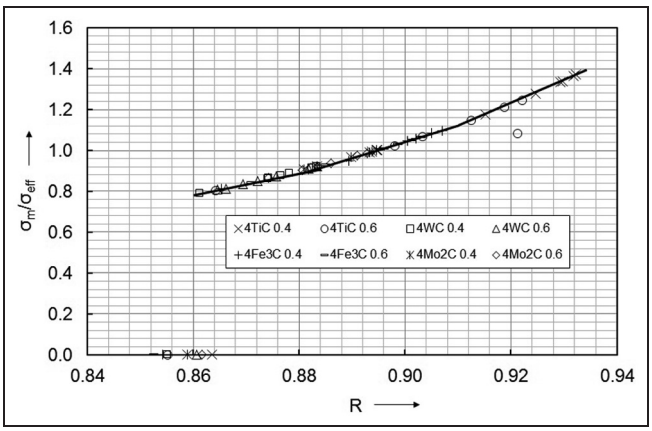

Figure 4. Relationship between stress ratio (σ_m/σ_{eff}) and relative density during hot deformation.

of 86%. As seen in Figure 2, the lateral deformation is highest in WC-reinforced aluminium composite followed by Mo_2C, then Fe_3C and then TiC composites. This means the effective closer of pores is higher in TiC-reinforced aluminium; therefore, it has higher density than any other composite tested.

Table 3 shows the equations obtained using polynomial best fit graphs with correlation values close to 1.0 for *R* versus ε_z. It can be seen that for zero height strain, a constant value of approximately 0.86 is obtained. This constant will change accordingly if the initial relative density is varied as the constant represents the initial relative density. Furthermore, the first-order value in Table 3 is found to be positive, meaning it is contributing to the densification linearly. Also, it is seen that the ε_z coefficient increases as the aspect ratio decreases, projecting that decreasing aspect ratio promotes densification. The second-order coefficient is found to be negative, and hence, its contribution is negative to densification and this negative contribution is more in lower aspect ratio preforms. However, the effect is less as the coefficient values are small in a range of 0–0.3 and is multiplied to the square of axial strain.

A plot has been presented as shown in Figure 3 between stress ratio, $\sigma_\theta/\sigma_{eff}$, and relative density, *R*, for two different initial aspect ratios, namely, 0.40 and 0.60, these plots being drawn for initial relative density of 86%. Furthermore, similar plots have been plotted for stress ratios σ_m/σ_{eff} and σ_z/σ_{eff} presented in Figures 4 and 5. From these plots, it can be seen the effect of aspect ratio and composition is nil on the characteristics behaviour. The respective stress ratio parameters increase as the relative density increases. The stress ratio behaviour can be found in two stages against densification, one from the start of densification till 0.912 relative density and the other from 0.912 relative density till the end of deformation. The slope is found to increase from stage 1 to stage 2 as high load is required to further deform the specimen as very little

Table 4. Actual bulged length for the respective composites at 0.40 height strain.

Composite		Bulge length (mm)
Al-4% TiC	0.4	1.052
	0.6	1.460
Al-4% Fe_3C	0.4	1.037
	0.6	1.394
Al-4% Mo_2C	0.4	0.980
	0.6	1.355
Al-4% WC	0.4	1.020
	0.6	1.305

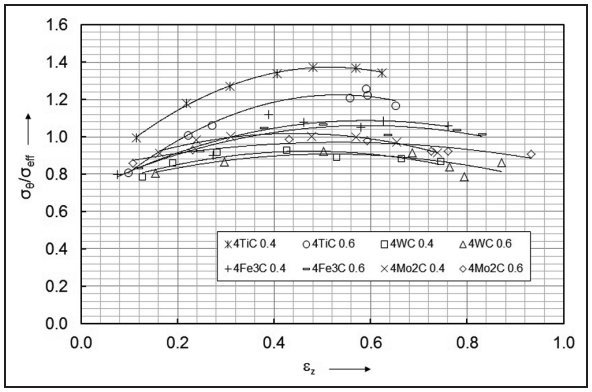

Figure 6. Relationship between stress ratio ($\sigma_\theta/\sigma_{eff}$) and axial strain during hot deformation.

pores are left towards the end of deformation. Against densification, the highest stress ratio value was achieved by TiC content composite followed by Fe_3C composite, Mo_2C composite and the lowest was WC-containing composite. Furthermore, the highest stress ratio parameter was obtained for smaller aspect ratio preform, which is true for all stress ratio preforms. This indicates that WC-containing composite and higher aspect ratio preform have further chance to be deformed provided the preform is free of cracks. The lateral deformation at the contact surface is lowest in TiC composite as seen in Figure 2 for any given height strain, indicating the bulging phenomenon is highest in TiC composite compared to Fe_3C, Mo_2C, and WC composites. The same can be seen in Table 4. Hence, the hoop stress is found to be highest in TiC composite compared to other composites. The same is true for the hydrostatic stress (σ_m/σ_{eff}) found to be highest in TiC composite.

A plot has been presented as shown in Figure 6 between stress ratio, $\sigma_\theta/\sigma_{eff}$, and axial strain for two different initial aspect ratios, namely, 0.40 and 0.60, these plots being drawn for initial relative density of 86%. Furthermore, similar plots have been plotted for stress ratios σ_m/σ_{eff} and σ_z/σ_{eff} presented in Figures 7 and 8. The effect of aspect ratio on the stress ratios, $\sigma_\theta/\sigma_{eff}$, σ_m/σ_{eff} and σ_z/σ_{eff} is literally nil when plotted against axial strain except for TiC-containing composite. The stress ratio parameters rise to a maximum

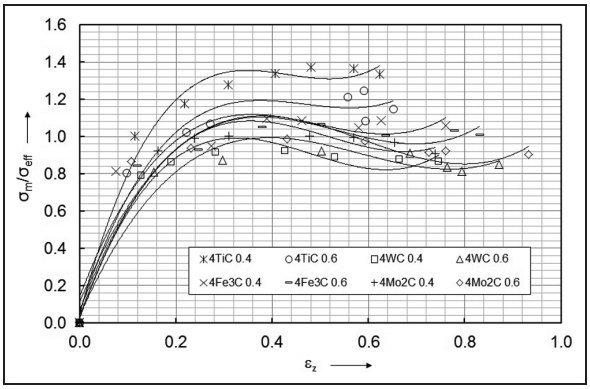

Figure 7. Relationship between stress ratio (σ_m/σ_{eff}) and axial strain during hot deformation.

value as the deformation starts and then settle for the steady-state stress for the rest of the deformation. However, all the stress ratios slightly lower towards the end mainly in Al-4% Mo_2C and Al-4% WC. For any given height strain, the hoop, mean and axial stress obtained are highest for TiC-containing compacts, followed by Fe_3C, Mo_2C and lowest for WC-containing compacts. This means WC-containing compacts can be further deformed provided it is free from defects. The TiC particulates impede the motion of dislocations more than Fe_3C, Mo_2C and WC particulates, and hence, the stress required for further plastic deformation for TiC composite is more than other composite. Due to this reason, the stress ratios, $\sigma_\theta/\sigma_{eff}$, σ_m/σ_{eff} and σ_z/σ_{eff}, are higher for TiC composite for any given true height strain. Furthermore, the polynomial curve fitting results with correlation values close to 1.0 for $\sigma_\theta/\sigma_{eff}$ versus ε_z are given in Table 5. It is found that the first-order values decrease while the second-order values increase with the increasing aspect ratio. Also, the first-order values that increase the hoop stress linearly are found to be higher in TiC composite compared to other composites.

A plot has been presented as shown in Figure 9 between formability index, β, and axial strain for two different initial aspect ratios, namely, 0.40 and 0.60, these plots being drawn for initial relative density of 86%. The formability of the TiC-containing compacts was found to be higher followed by Fe_3C and Mo_2C composites. WC-containing compacts showed lowest formability ratio for any given axial strain. For any given axial strain, the relative density is found to be highest in TiC composite (Figure 1), meaning the porosity level is low and hence the reason for high formability index for TiC composite. The true hydrostatic stress (σ_m/σ_{eff}) is higher in TiC composite than the true effective stress compared to Fe_3C, Mo_2C and WC composites (Figure 7) and is the reason for high formability in TiC composite. The compositions are calculated using weight percentage and TiC particulate being the lowest weight followed by Fe_3C, Mo_2C and WC (Table 2). This means the amount of smaller and fine

Table 5. Polynomial curve fitting result $-\sigma_\theta/\sigma_{eff}$ versus ε_z.

Al-4TiC	0.4	$\sigma_\theta/\sigma_{eff} = -2.3226\varepsilon_z^2 + 2.3946\varepsilon_z + 0.7555$	$R_c^2 = 0.9989$
	0.6	$\sigma_\theta/\sigma_{eff} = -2.209\varepsilon_z^2 + 2.3554\varepsilon_z + 0.5968$	$R_c^2 = 0.9922$
Al-4Mo_2C	0.4	$\sigma_\theta/\sigma_{eff} = -1.183\varepsilon_z^2 + 1.0494\varepsilon_z + 0.7852$	$R_c^2 = 0.9991$
	0.6	$\sigma_\theta/\sigma_{eff} = -0.5314\varepsilon_z^2 + 0.5667\varepsilon_z + 0.8191$	$R_c^2 = 0.9951$
Al-4Fe_3C	0.4	$\sigma_\theta/\sigma_{eff} = -1.138\varepsilon_z^2 + 1.3437\varepsilon_z + 0.6908$	$R_c^2 = 0.9949$
	0.6	$\sigma_\theta/\sigma_{eff} = -1.0076\varepsilon_z^2 + 1.1931\varepsilon_z + 0.7070$	$R_c^2 = 0.9920$
Al-4WC	0.4	$\sigma_\theta/\sigma_{eff} = -0.9698\varepsilon_z^2 + 0.9169\varepsilon_z + 0.7061$	$R_c^2 = 0.9950$
	0.6	$\sigma_\theta/\sigma_{eff} = -0.7433\varepsilon_z^2 + 0.7681\varepsilon_z + 0.7089$	$R_c^2 = 0.9961$

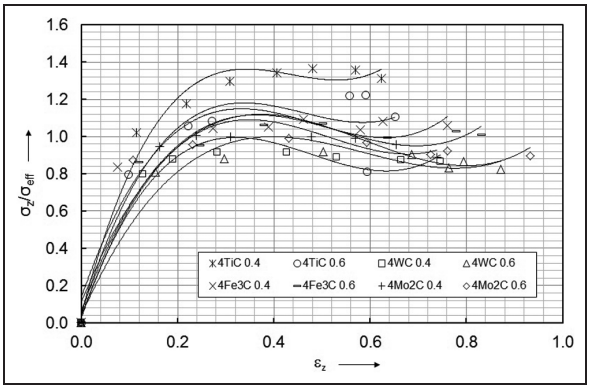

Figure 8. Relationship between stress ratio (σ_z/σ_{eff}) and axial strain during hot deformation.

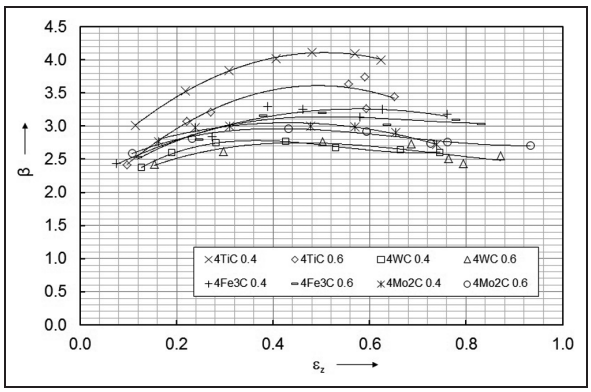

Figure 9. Relationship between formability stress ratio and axial strain during hot deformation.

Table 6. Polynomial curve fitting result $-\beta$ versus ε_z.

Al-4TiC	0.4	$\beta = -7.1569\varepsilon_z^2 + 7.2373\varepsilon_z + 2.2798$	$R_c^2 = 0.9979$
	0.6	$\beta = -7.5964\varepsilon_z^2 + 7.4891\varepsilon_z + 1.7654$	$R_c^2 = 0.9971$
Al-4Mo_2C	0.4	$\beta = -3.4469\varepsilon_z^2 + 2.9723\varepsilon_z + 2.3094$	$R_c^2 = 0.9965$
	0.6	$\beta = +3.8739\varepsilon_z^3 - 7.7228\varepsilon_z^2 + 4.3776\varepsilon_z + 2.1973$	$R_c^2 = 0.9943$
Al-4Fe_3C	0.4	$\beta = -3.3318\varepsilon_z^2 + 3.8454\varepsilon_z + 2.1501$	$R_c^2 = 0.9928$
	0.6	$\beta = +4.6303\varepsilon_z^3 - 9.5042\varepsilon_z^2 + 6.0699\varepsilon_z + 1.9044$	$R_c^2 = 0.9913$
Al-4WC	0.4	$\beta = +3.1557\varepsilon_z^3 - 7.1485\varepsilon_z^2 + 4.5426\varepsilon_z + 1.8638$	$R_c^2 = 0.9931$
	0.6	$\beta = +9.71\varepsilon_z^3 - 15.516\varepsilon_z^2 + 7.4421\varepsilon_z + 1.6901$	$R_c^2 = 0.9963$

pores present in Al-4TiC composite is more than other composites. The effective closure of pores is more in TiC composite during hot upsetting increasing the densification (Figure 1), and hence, for the same reason, the formability ratio is higher in TiC composite.

The polynomial curve fitting results with correlation values close to 1.0 for β versus ε_z are given in Table 6. Second-order and third-order polynomial fits are used to obtain the correlation values near unity; however, the constant, first- and second-order values are upmost important. A constant formability stress value was obtained for zero axial strain. This constant value is approximated to be 2.0 ± 0.3. It is found that the first-order values increase while the second-order values and constant values decrease with the increasing aspect ratio, and hence, the formability of the material decreases with increasing aspect ratio. The first-order values are found to be positive while the second-order values are found to be negative revealing that at the initial stages of deformation for low enhancement in axial strain the formability index is profound.

Furthermore, a plot has been presented as shown in Figure 10 between formability index, β, and relative density for two different initial aspect ratios, namely, 0.40 and 0.60, these plots being drawn for initial relative density of 86%. The effect of aspect ratio and composition showed nil effect on the formability behaviour against relative density; however, the final formability ratio achieved against relative density and axial strain is also important. In view of this, a graph of formability index at fracture and axial strain at fracture is plotted as shown in Figure 11. The axial strain at fracture is found to be higher for higher aspect ratio preforms in

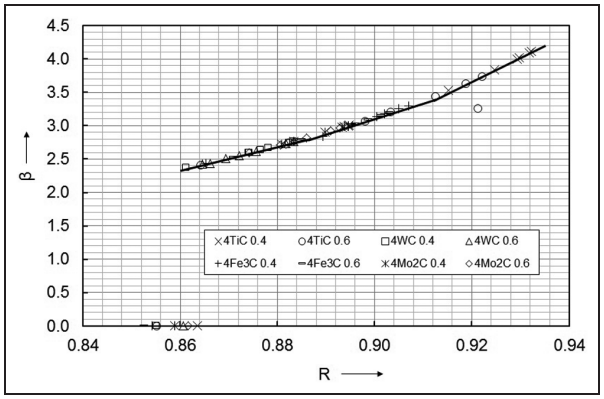

Figure 10. Relationship between formability stress ratio and relative density during hot deformation.

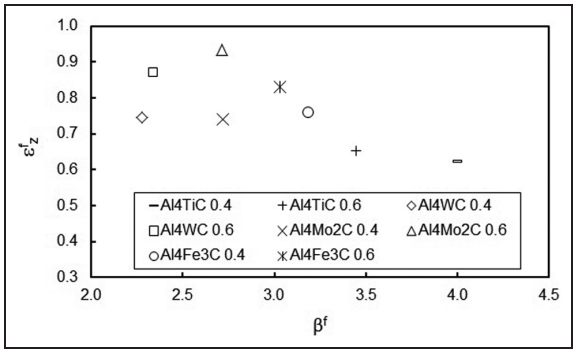

Figure 11. Relationship between fracture strain (ε_z^f) and formability stress index at fracture (β^f) during hot deformation.

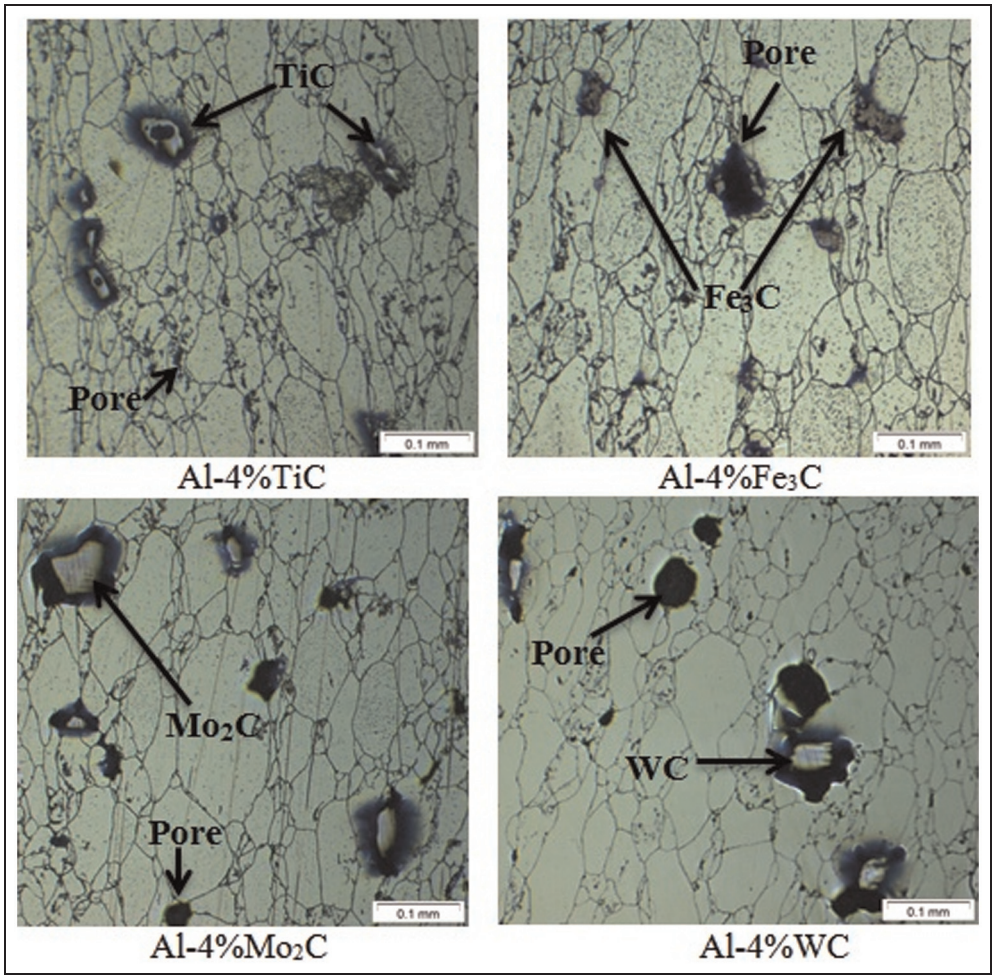

Figure 12. Optical micrographs of various sintered aluminium composites with 50% deformation at the centre.

comparison to lower aspect ratio preforms. There is an inverse relationship between fracture strain and fracture formability stress index as shown in Figure 11. This effect is more in lower aspect ratio preforms. WC-containing compacts showed higher fracture strain followed by Mo_2C composite, then Fe_3C composite and lowest fracture strain for TiC composites. Also, the number of carbide particles is higher in Al-4% TiC composite compared to other composites prepared, meaning the amount of pores is higher in Al-4% TiC leading to lower fracture strain.

Furthermore, to understand the deformation behaviour of Al-4% TiC, Al-4% Fe_3C, Al-4% Mo_2C and Al-4% WC, the microstructure view of 100× magnification is shown in Figures 12 and 13, respectively. Particularly, the view was selected one at the centre (Figure 12) and other one at the extreme diametric side of each of the preforms (Figure 13) in order to view the

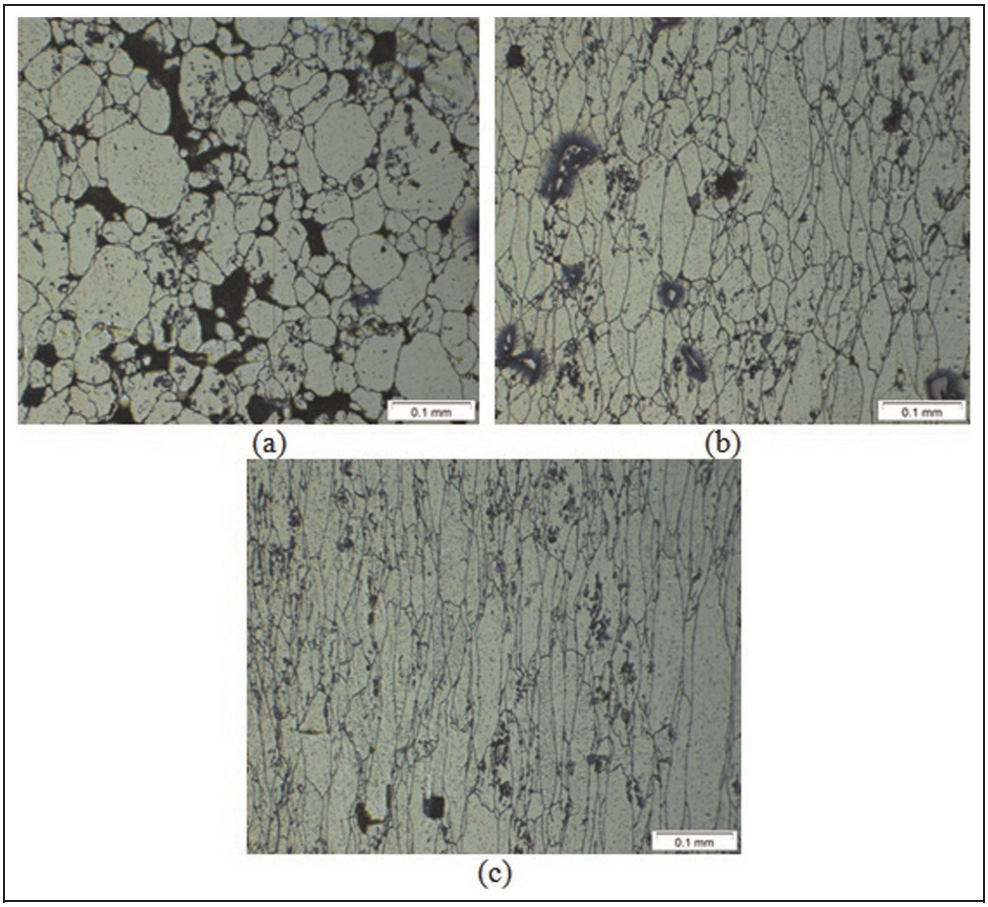

Figure 13. Optical micrographs of Al-4% TiC at the diametrical end: (a) undeformed, (b) medium deformed and (c) fully deformed.

presence of porosities. The upsetting axis is horizontal in Figures 12 and 13. The grain boundaries are clear and straight. As seen in Figure 12, less number of pores is found in TiC and Fe_3C when compared to Mo_2C and WC composites; however, more equi-axed grains are found in Mo_2C and WC composites compared to TiC and Fe_3C composites. The reduction in pores from undeformed specimen (green compact) to medium deformed and full deformed (at fracture) can be seen in Figure 13. The grains are equi-axed form in the green compact (Figure 13(a)), and then during deformation process, the grains elongate in the direction perpendicular to the compression direction as seen in Figure 13(c). The pores at the centre of the specimen are found to be spherical shape (Figure 12) while at the diametric ends are mainly elongated (Figure 13).

Conclusion

The design of preform shape and die are very important such that the final part produced is free from defects (fracture) since there is little possibility that the cracks can be arrested during the repressing stage of the deformation. Accordingly, the major conclusions have been drawn that are as follows.

- The TiC-containing compacts showed better densification, thereby the stress formability index of the preform followed by Fe_3C, then Mo_2C and lowest for WC-containing compacts. However, it limited height strain to fracture.
- Decreasing the aspect ratio facilitates uniform deformation resulting in improved densification and formability behaviour of the preform; however, it limits the height strain to fracture.
- The variation in aspect ratio and hard carbide particles in aluminium composite made nil impact in the stress ratio behaviour against densification, however, against true axial strain induced is prominent.
- The amount of pores and grain structure varies significantly in the composites tested at 50% deformation. The final grain distribution reveals strong orientation along the compression direction, resulting in a fibre structure.
- The relationship between stress ratio and formability against axial strain and relative density is established using polynomial curve fitting results.

Acknowledgement

The authors would like to acknowledge the help rendered by Mr Sanjay Singh, Mr Shiu Prasad and Mr Navneel Prasad, Metal Workshop Technicians at the University of the South Pacific, during the experimental phase of this project.

Declaration of conflicting interests

The authors declare that there is no conflict of interest.

Funding

This research received no specific grant from any funding agency in the public, commercial, or not-for-profit sectors.

References

1. Sahin Y. Preparation and some properties of SiC particle reinforced aluminium alloy composites. *Mater Design* 2003; 24: 671–679.
2. Sahin Y. The effect of sliding speed and microstructure on the dry wear properties of metal matrix composite. *Wear* 1998; 214: 98–106.
3. Derakhshandeh RH and Jahromi AJ. An investigation on the capability of equal channel angular pressing for consolidation of aluminum and aluminum composite powder. *Mater Design* 2011; 32: 3377–3388.
4. Zebarjad SM and Sajadi SA. Dependency of physical and mechanical properties of mechanical alloyed Al–Al_2O_3 composite on milling time. *Mater Design* 2007; 28: 2113–2120.
5. Fogagnolo JB, Velasco F, Robert MH, et al. Effect of mechanical alloying on the morphology, microstructure and properties of aluminium matrix composite powders. *Mat Sci Eng A: Struct* 2003; 342: 131–143.
6. Prabhu B, Suryanarayana C, An L, et al. Synthesis and characterization of high volume fraction Al–Al_2O_3 nanocomposite powders by high energy milling. *Mat Sci Eng A: Struct* 2006; 425: 192–200.
7. Sheibani S and Fazel MN. In situ fabrication of Al-TiC metal matrix composites by reactive slag process. *Mater Design* 2007; 28: 2373–2378.
8. Zhong L, Xu Y, Hojamberdiev M, et al. In situ fabrication of titanium carbide particulates-reinforced iron matrix composites. *Mater Design* 2011; 32: 3790–3795.
9. Lui CY, Wang Q, Jia YZ, et al. Evaluation of mechanical properties of 1060-Al reinforced with WC particles via warm accumulative roll bonding process. *Mater Design* 2013; 43: 367–372.
10. Selvakumar N, Ganesan P, Radha P, et al. Modelling the effect of particle size and iron content on forming of Al-Fe composite preforms using neural network. *Mater Design* 2007; 28: 119–130.
11. Taha MA, El-Mahallawy NA and El-Sabbagh AM. Some experimental data on workability of aluminium-particulate-reinforced metal matrix composites. *J Mater Process Tech* 2008; 202: 380–385.
12. Rajeshkannan A. Workability studies on cold upsetting of sintered copper alloy preforms. *Mater Res* 2010; 13: 457–464.
13. Narayanasamy R, Ramesh T and Pandey KS. Some aspects on workability of aluminium-iron powder metallurgy composite during cold upsetting. *Mat Sci Eng A: Struct* 2005; 391: 418–426.
14. Abdel-Rahman M and El-Sheikh MN. Workability in forging of powder metallurgy compacts. *J Mater Process Tech* 1995; 54: 97–102.
15. El-Domiatry A and Shaker M. A note on the workability of porous-steel preforms. *J Mater Process Tech* 1991; 25: 229–233.
16. Spigarelli S, Cerri E, Cavaliere P, et al. An analysis of hot formability of the 6061 + 20% Al_2O_3 composite by means of different stability criteria. *Mat Sci Eng A: Struct* 2002; 327: 144–154.
17. Rahimian M, Ehsani N, Parvinb N, et al. The effect of particle size, sintering temperature and sintering time on the properties of Al–Al_2O_3 composites, made by powder metallurgy. *J Mater Process Tech* 2009; 209: 5387–5393.
18. Dannininger H, Jangg G, Weiss B, et al. Microstructure and mechanical properties of sintered iron. Part I: basic consideration and review of literature. *Powder Metall Int* 1993; 25: 170–173.
19. Lee SR, Lee YK, Park CH, et al. A new method of preform design in hot forging by using electric field theory. *Int J Mech Sci* 2002; 44: 773–792.
20. Solhjoo S. Analysis of flow stress up to the peak at hot deformation. *Mater Design* 2009; 30: 3036–3040.
21. Kuhn HA and Downey CL. How flow and fracture affect design of preforms for powder forging. *Int J Powder Metall Powder Tech* 1974; 10: 59–66.
22. Shima S and Oyane M. Plasticity theory for porous metals. *Int J Mech Sci* 1976; 18: 285–291.
23. Green RJ. A plasticity theory for porous solids. *Int J Mech Sci* 1972; 14: 215–224.
24. Narayanasamy R, Senthilkumar V and Pandey KS. Effect of titanium carbide particle addition on the densification behaviour of sintered P/M high strength steel preforms during cold upset forming. *Mat Sci Eng A: Struct* 2007; 456: 180–188.
25. Narayanasamy R, Ponalagusamy R and Subramanian KR. Generalized yield criteria of porous sintered powder metallurgy metals. *J Mater Process Tech* 2001; 110: 182–185.
26. Narayanasamy R, Anandakrishnan V and Pandey KS. Effect of geometric work-hardening and matrix work-hardening on workability and densification of aluminium–3.5% alumina composite during cold upsetting. *Mater Design* 2008; 29: 1582–1599.
27. Vujovic V and Shabaik AH. A new workability criterion for ductile materials. *J Eng Mater: T ASME* 1986; 108: 245–249.
28. Doraivelu SM, Gegel HL, Gunasekara JS, et al. A new yield function for compressible P/M materials. *Int J Mech Sci* 1984; 26: 527–535.
29. Ko BC, Park GS and Yoo YC. The effects of SiC particle volume fraction on the microstructure and hot workability of SiC_p/AA 2024 composite. *J Mater Process Tech* 1999; 95: 210–215.
30. Narayanasamy R, Senthilkumar V and Pandey KS. Some features on hot forging of powder metallurgy sintered high strength 4% titanium carbide composite steel preforms under different stress state conditions. *Mater Design* 2008; 29: 1380–1400.
31. Narayanasamy R, Senthilkumar V and Pandey KS. Some aspects of workability studies on hot forging of sintered high strength 4% titanium carbide composite steel preforms. *Mat Sci Eng A: Struct* 2006; 425: 121–130.
32. Narayanasamy R, Ramesh T and Pandey KS. Workability studies on cold upsetting of Al–Al_2O_3 composite material. *Mater Design* 2006; 27: 566–575.

33. Qin XP and Hua L. Deformation and strengthening of sintered ferrous material. *J Mater Process Tech* 2007; 188: 694–697.
34. Han HN, Oh KH and Lee DN. Analysis of forging limit for sintered porous metals. *Scripta Metall Mater* 1995; 32: 1937–1944.
35. Lewis RW and Khoei AR. A plasticity model for metal powder forming processes. *Int J Plasticity* 2001; 17: 1659–1692.

Appendix I

Notation

$d\varepsilon_z$	plastic axial strain increment
$d\varepsilon_\theta$	plastic hoop strain increment
R	relative density
α	Poisson's ratio
β	stress formability factor
β^f	stress formability factor at fracture
ε_{eff}	effective strain
ε_z	true axial strain
ε_z^f	true axial strain to fracture
ε_θ	true hoop strain
σ_{eff}	effective stress
σ_m	hydrostatic stress
σ_r	radial stress
σ_z	axial stress
σ_θ	hoop stress